Materials Chemistry and Physics 137 (2013) 1012–1020

Contents lists available at SciVerse ScienceDirect

Materials Chemistry and Physics

journal homepage: www.elsevier.com/locate/matchemphys

LDA + U and GGA + U studies of Al-rich and bulk goethite (α-FeOOH)

Silvia A. Fuente [a], Patricia G. Belelli [b,*], Norberto J. Castellani [b], Marcelo Avena [a]

[a] INQUISUR, Departamento de Química, Universidad Nacional del Sur, Av. Alem 1253, Bahía Blanca B8000CP, Argentina
[b] IFISUR, Grupo de Materiales y Sistemas Catalíticos, Departamento de Física, Universidad Nacional del Sur, Av. Alem 1253, Bahía Blanca B8000CP, Argentina

HIGHLIGHTS

- We studied electronic and structural properties of bulk goethite and Al-rich goethite.
- The goethite is well described with the GGA + U level using the $U_{eff} = 6$ eV value.
- The Al-rich goethite model has different magnetic structures with similar energies.
- The isomorphic substitution of Fe by Al atom in goethite results in a lattice contraction.

ARTICLE INFO

Article history:
Received 1 September 2011
Received in revised form
10 October 2012
Accepted 8 November 2012

Keywords:
Oxides
Ab initio calculations
Electronic structure
Magnetic structures

ABSTRACT

The electronic and structural properties of bulk goethite and Al-rich goethite were studied on the basis of spin-polarized DFT at the LDA + U and GGA(PW91) + U levels. Firstly, the periodic model of bulk goethite was optimized varying the value of U_{eff}. Considering all the results obtained we can conclude that the bulk goethite described at the GGA + U level with $U_{eff} = 6$ eV gives us the better agreement with different physical properties. The results of magnetic moments of Fe ions, the DOS analysis and the Bader atomic charges identify goethite as an antiferromagnetic Fe(III) compound. For Al-rich goethite the GGA + U ($U_{eff} = 6$ eV) approach was used. The isomorphous substitution of one Fe ion with Al ion produces the reduction of the cell parameters with respect to the bulk goethite. Regarding the magnetic ordering, it was observed that Fe atoms surrounding the Al atom must have the same spin projection, i.e., spin-up or -down. The charge density was changed with the addition of Al ion, producing a depletion where the ion is located and some electron redistribution in the zone of the oxygen atoms surrounding the Al ion. This behavior produces some small magnetization in these O ions.

1. Introduction

Goethite (α-FeOOH) is one of the most important iron minerals found in soils and sediments. It crystallizes in the orthorhombic system with a space group that was recently changed from *Pbnm* to *Pnma* according to the *International Tables of Crystallography* [1]. The geometrical structure of goethite has a hexagonally close packed array of O atoms slightly distorted with the Fe atoms occupying two-thirds of the octahedral sites. It has two independent O atoms; one is surrounded by three Fe atoms whereas the other one is protonated and surrounded by two Fe atoms. Below the Néel temperature (130 ± 2 °C), goethite is an antiferromagnetic (AFM) insulator, i.e., it will show this behavior at ambient temperature [2]. The goethite is a highly reactive mineral and plays an important role in environmental processes due to its strong affinity toward different contaminants. This reactivity is directly associated with the surface structure and the composition of the mineral particles. The most stable surface structures of goethite are (110) and (210) [82]. The nature and properties of this oxy-hydroxide are also relevant in geochemistry, mineralogy and in planetary science because goethite was identified on the surface of Mars [3]. Over the past 20 years many much experimental efforts using different techniques have been performed on bulk goethite to describe its structural, magnetic and electronic properties. These studies comprise from natural minerals to synthesized samples and, in the more recent experiments, goethite was exposed to high pressures and temperatures [4–6]. Moreover, goethite is a component in new nanocomposite materials for magnetic applications [7].

Usually, natural α-FeOOH has incorporations of different foreign elements; for example, soil goethites may contain substantial amounts of Al (up to 33 mol%) by the substitution of Fe^{3+} ion in the octahedral sites. It is commonly assumed that the Al incorporation into the goethite crystal takes place through an isomorphous ionic substitution of Fe yielding strain in the goethite structure [8–10].

* Corresponding author. Tel.: +54 291 4595141; fax: +54 291 4595142.
E-mail address: pbelelli@plapiqui.edu.ar (P.G. Belelli).

0254-0584/$ – see front matter © 2012 Elsevier B.V. All rights reserved.
http://dx.doi.org/10.1016/j.matchemphys.2012.11.017

This strain could be associated with the presence of shorter Al–O bonds, producing the decrease of at least one of the unit cell parameters of goethite [10–13]. The axis along *a*-vector is the most sensitive parameter due to the presence of excess structural OH related to Al-substitution [14,15]. On the other hand, the substitution of a paramagnetic ion (Fe^{3+}) for a diamagnetic ion (Al^{3+}) modifies the magnetic interactions and thereby lowers the Néel temperature. About 12 mol% Al-substitution is sufficient to lower the Néel temperature of goethite below ambient temperature [16]. The doping of this hydroxide with Mg or B has been considered in relation to adsorptive properties [17,18].

The presence of Al in goethite structures was discovered seventy years ago. Subsequently, several authors have confirmed the fact that natural goethites rarely exist in pure state. Recent experimental studies showed that the Al–goethites are rarely formed with Al contents higher than 20 mol% [19]. These results and others found in literature reflect the dependency on the experimental synthesis conditions to obtain the desired Al content for the goethite structure.

From the theoretical point of view, a few works about structural, magnetic and electronic properties of goethite can be found in the open literature, including related oxides and oxy-hydroxides such as diaspore (α-AlOOH), boehmite (γ-AlOOH), hematite (α-Fe_2O_3), etc. [20–25]. Specifically, goethite was modeled with two different approaches within the framework of DFT (Density Functional Theory), using a cluster model of the surface as well as a periodic slab [26–33].

It is well known that the DFT within the standard local density approximation (LDA) or the generalized gradient approximation (GGA) for the exchange and correlation functionals fails to predict the proper electronic ground state of magnetic materials with strong electronic correlations of the *d* and *f* valence electrons in transition and lanthanide metal atoms [23,24,34,35]. In many cases these functionals describe an insulating compound as a conductor one, at the LDA level, or with a too small band gap, at the GGA level, indicating their erroneous metallic or semiconductor behaviors, respectively [23,36]. Many different methods have been proposed to overcome this limitation of standard DFT approaches. One of them is to add an effective on-site repulsion term (*U*) of a Coulombic-type to the LDA Hamiltonian. However, the term may vary for the same element in different polymorphs, and needs to be adjusted for each structure under investigation. The value of *U* is a matter of debate because the correct value is strongly influenced by the better approach of the calculated observables in comparison with the experimental values. Cococcioni et al. [37,38] developed a linear response approach which was employed by other authors for different oxides [32,39–42]. However, it was observed that the value obtained by this procedure does not provide in some cases the correct *U* in order to have a well fit of experimental observables [36]. Besides, some authors found that the appropriated *U* value does not predict simultaneously the structural and electronic properties [43–45]. Furthermore, its value also changes for the exchange and correlation approaches and for the type of functional used. For example in ceria oxides, different *U* values were recommended for GGA using PBE [43] and PW91 [44] functional.

This work has two objectives. First, to make a systematically study of several physical properties of bulk goethite by performing DFT calculations with the inclusion of an effective on-site repulsion term, and afterwards, to extend this methodology to the case of bulk goethite doped with Al, where besides to structural, magnetic and electronic properties, some relevant vibrational properties were considered.

2. Computational details

All the calculations described in this paper have been performed on the basis of spin-polarized DFT using the *Vienna Ab-Initio Simulation Package* (VASP) [46–48]. Plane wave basis sets were used to solve the Kohn–Sham equations. The electron–ion interactions were described by the projector-augmented wave method (PAW). The PAW technique is a frozen core all-electron method that uses the exact shape of the valence wave functions instead of pseudo-wave functions [49,50]. The following valence electron configurations were employed for the PAW pseudopotentials: d^7s^1 for Fe atoms, s^2p^4 for O atoms, s^1 for H atoms and s^2p^1 for Al atom.

Two different approximations to treat exchange and correlation were applied: (i) the LDA + *U* and (ii) GGA + *U*, following the approach of Dudarev for different values of *U* [51]. Both methods require specification of an on-site exchange interaction parameter *J* and an on-site Coulomb interaction parameter *U*. However in the most widely used implementation employed in the published works, the results depend only on the difference between these values, i.e., the effective *U* (U_{eff}). The implementation of the DFT + *U* approach within VASP was carefully described elsewhere [45]. The GGA electron exchange and correlation effects were described using the Perdew and Wang functional (PW91) [52,53]. Taking into account that LDA + *U* and GGA + *U* could yield multiple metastable states corresponding to different occupations of Fe 3*d* states, a set of test calculations were performed with the procedure described by Meredig et al. [54] which is based on the Liechtenstein et al. approach [55]. The resulting geometrical parameters for goethite and Al-doped goethite do not change and the total energy values show only a slight difference with respect to the Dudarev approach (about 0.02 eV $cell^{-1}$).

As the orthorhombic primitive cell of goethite contains four FeOOH formula units (see Fig. 1), considerable computational effort is required to obtain reasonable results concerning the crystalline, electronic, and magnetic structures of bulk goethite. The cutoff energy of 450 eV was determined taking into account the converged results of the energies with respect to basis set size. The Brillouin zone was performed on a grid of 4 × 2 × 6 Monkhorst–Pack special *k*-points.

In this study, two different methods of structural relaxation were used for bulk goethite. Though the atomic positions of all

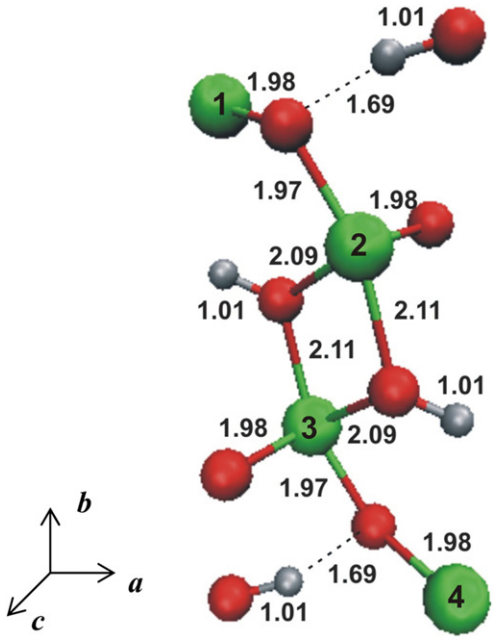

Fig. 1. Optimized unit cell of goethite with GGA + *U* (U_{eff} = 6). Red, green and gray balls correspond to O, Fe and H atoms, respectively. The *a*, *b* and *c* unit cell vectors have been indicated. Distances between atoms are expressed in Armstrongs (Å). (For interpretation of the references to color in this figure legend, the reader is referred to the web version of this article.)

atoms were allowed to relax in both methods, in the first one the three cell parameters were independently modified, whereas in the second one these parameters are simultaneously modified in a linear relationship (Homothetic relaxation, named H). In both methods, the incompleteness of the plane wave basis set with respect to the volume changes (Pulay stress) was minimized with an increase of 30% of the cutoff energy found initially for the bulk goethite. Optimized parameters were found when the forces on atoms were smaller than 0.01 eV $Å^{-1}$.

The bulk modulus was determined by fitting the volume vs. energy relationship with the Birch–Murnaghan equation of states. The local electronic density of states (LDOS) have been calculated with a higher *k*-point mesh of $4 \times 2 \times 6$, and the band gap values were extracted from these results. The numerical calculation of the second derivatives of the potential energy surface within the harmonic approach provided the vibrational frequencies and corresponding normal modes. A geometrical displacement of 0.02 Å was used for all vibrational calculations.

3. Results and discussion

3.1. Bulk goethite

In almost all published papers, the exchange and correlation functionals reported were described by GGA, but further authors found for other oxides the importance to describe the geometrical parameters with the LDA approximation [36]. For this reason and in order to have a wider approximation to this system, the bulk goethite was tested with both LDA + *U* and GGA + *U* methods, changing the U_{eff} values from 0 to 7 eV.

Although the bulk goethite is an antiferromagnetic material below the Néel temperature, different possibilities for the magnetic configurations arrangement were tested: a nonmagnetic phase (non-spin polarized configuration), a ferromagnetic phase, and three antiferromagnetic phases, changing the localization of up and down spin projections of Fe atoms within the cell. In this way we found that for both functionals the most stable magnetic phase was that of the AFM arrangement, which corresponds to the situation where each Fe atom is surrounded by other two Fe atoms with opposite magnetic moments along the *b*-vector axis. These results are in agreement with experiments [2] and with previous calculations reported by other authors using the functional form of Perdew, Burke and Enzerhof (PBE) [32].

In Fig. 2, the optimized cell parameters *a*, *b* and *c* are displayed as a function of U_{eff} in the range 0–7 eV. For comparison, several experimental values found in the literature were included as dotted horizontal lines. A decreasing trend is observed for both DFT levels. At the LDA + *U* level, the cell parameter values are always lower than the corresponding experimental data (nearly 2–3% lower). On the other hand, at the GGA + *U* level, the parameters are slightly overestimated for low U_{eff} values and they are very close to the experimental values for large U_{eff}. Regarding the methodology used for the geometry optimization, it does not have a significant effect on the lattice parameters. The internal Fe–O and Fe–OH (OH is the oxygen atom linked with a hydrogen atom) distances show slight modification with different U_{eff} values. The distances have a negligible variation from $U_{eff} = 3$ to 7 eV; in case of LDA + *U*, the Fe–O and Fe–OH distances are 1.94 Å and 2.04 Å, whereas for GGA + *U* they are 1.97 Å and 2.11 Å, respectively. We notice that the obtained values are similar to the experimental ones (Fe–O: 1.89 and 1.95 Å and for Fe–OH: 2.09 and 2.12 Å, in Refs. [56,57], respectively). In case of standard GGA and LDA these distances decrease up to 0.06 Å and 0.13 Å, respectively. Notice that the geometrical parameters are increasing function of the U_{eff} parameter, as it was observed in other calculations; nevertheless, for U_{eff} greater than 3 it shows a smooth decreasing behavior.

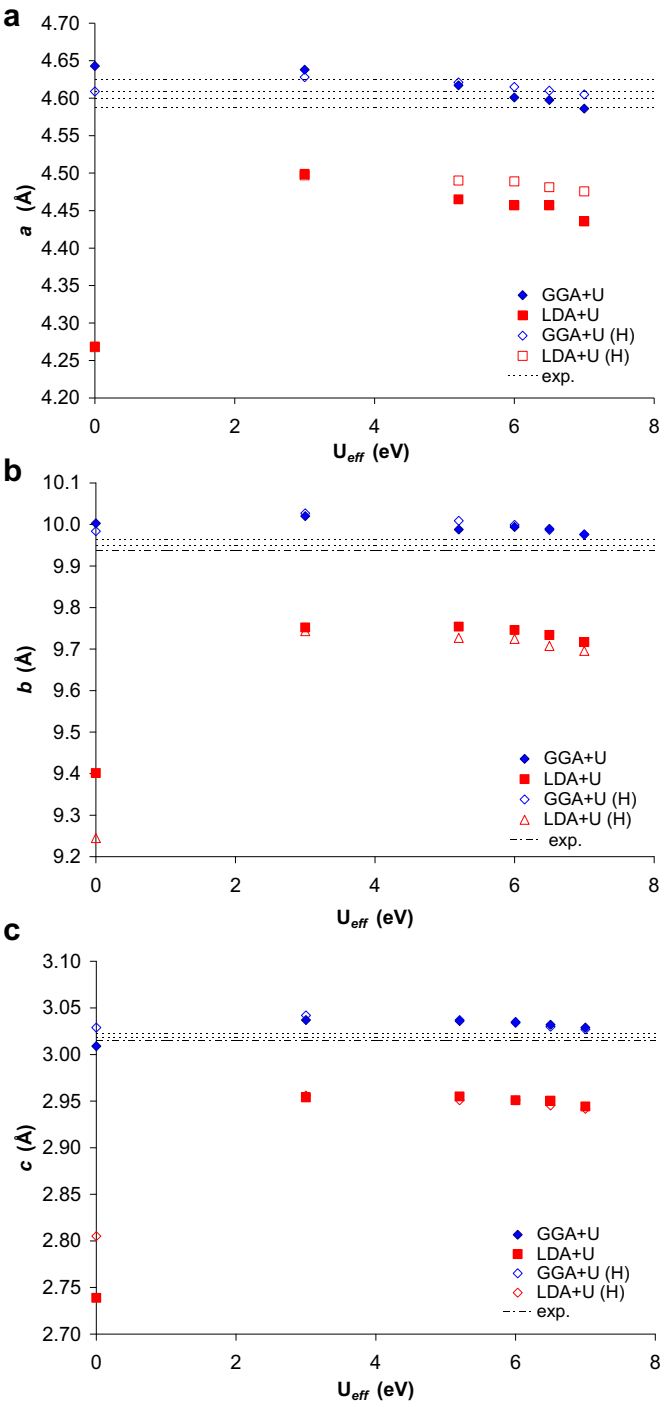

Fig. 2. Dependence of *a*, *b* and *c* lattice parameters of FeOOH on U_{eff} value. For each U_{eff} value, two types of optimizations were performed: one considering a free optimization and the second one for Homothetic (H) optimization. Experimental values for the lattice parameters found in the literature are depicted by dotted lines.

The results of this decreasing behavior can be rationalize considering that for both LDA + *U* and GGA + *U* the Fe atoms acquire a more ionic character than in the case of standard LDA and GGA (see later comments), producing a smaller cell volume. As comparison, the Fe–O distances in FeO, about 2.17 Å, are larger than in Fe_2O_3, about 2.06 Å. This point was carefully tested for some U_{eff} values using the PBE functional. The resulting lattice parameters follow the same trend that was observed using PW91 method.

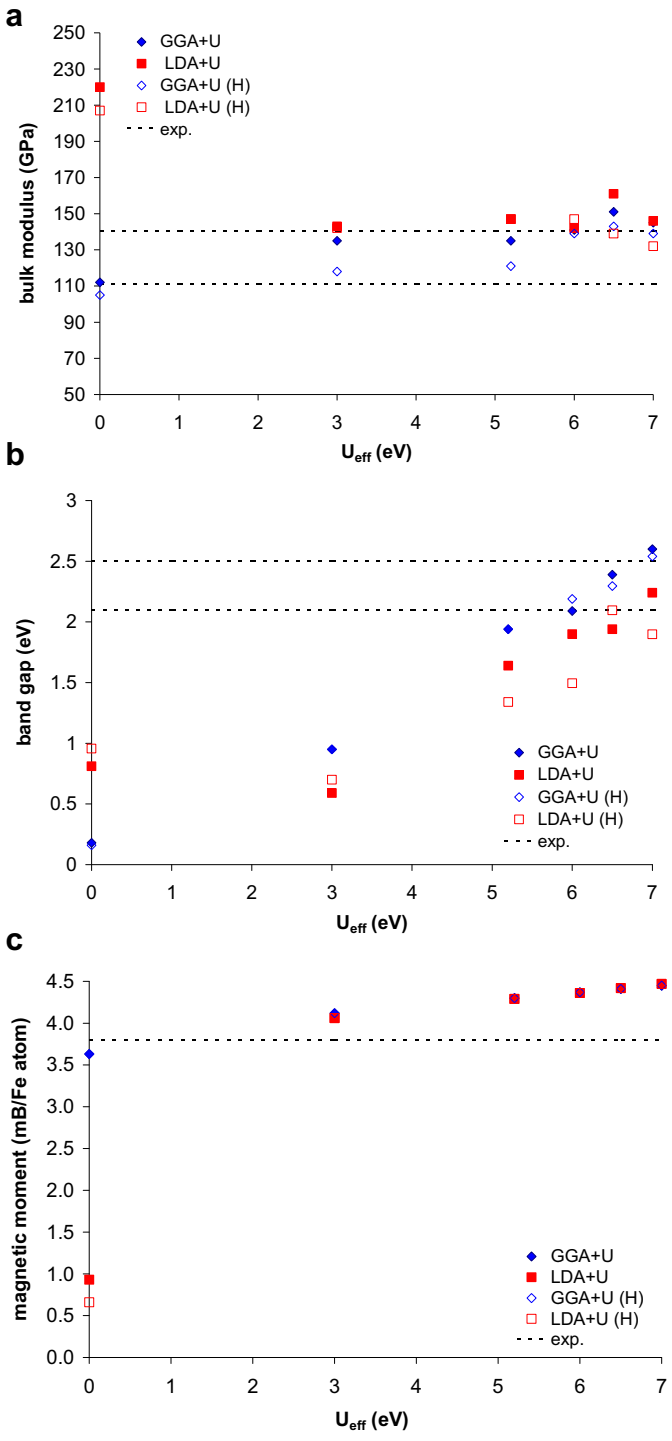

Fig. 3. (a) Calculated bulk moduli for FeOOH (in GPa), (b) band gap (in eV) and (c) magnetic moments (in μ_B/Fe atom) for GGA + U(PW91) and LDA + U varying the U values in the range 0–7 eV. For each U_{eff} value, the free and Homothetic (H) optimizations were performed. Experimental values are depicted by dotted lines.

In Fig. 3(a) the results of the bulk moduli for bulk goethite performed at LDA + U and GGA + U levels are shown. Experimental values of bulk modulus are scarcely found in open literature and they are very dispersed in the range from 111 to 140 GPa [5,6]. At the standard LDA level (with U_{eff} = 0 eV), an extremely high value was obtained, compatible with the small cell parameters predicted in this case. When the U_{eff} is not zero, the bulk modulus values are smaller and close to the experimental ones, but they do not show

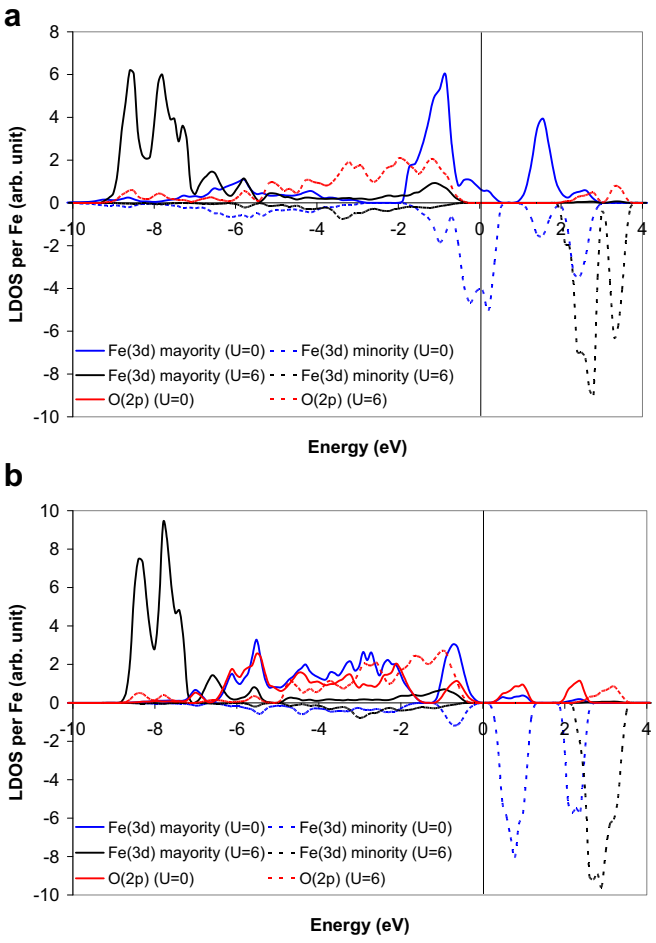

Fig. 4. LDOS localized on Fe and O atoms of FeOOH for: (a) LDA and LDA + U (U_{eff} = 6 eV); (b) GGA and GGA + U (U_{eff} = 6 eV). The zero value of energy corresponds to the Fermi level. Negative numbers on the LDOS axis indicate the spin-down polarization.

a clear tendency. The results corresponding to GGA + U present a different behavior. For the standard GGA + U, the bulk modulus is much lower than the corresponding value obtained with LDA. Introducing a non zero U_{eff}, the bulk modulus increase with a lineal trend between the experimental data. A recent theoretical work of goethite using PBE functional and ultrasoft pseudopotentials showed that the bulk modulus value obtained with GGA + U (U_{eff} = 5.2 eV) reproduced the lower experimental value [32], but all the cell parameters were higher than our results.

Taking into account the results for the geometrical parameters and bulk moduli above commented, we can infer that using GGA + U with U_{eff} = 6.0 eV a reasonable representation of elastic properties at the equilibrium is obtained. We notice that, previously, Rollmann et al. [23] performed a detailed description of the geometric and electronic properties of hematite with a U_{eff} value of 4 eV. Kubicki et al. [58] used the same U_{eff} value for the goethite structure, focusing their interest on thermodynamic properties. On the other hand, Russell et al. [32] found, with a self-consistent method, a U_{eff} value of 5.2 eV for goethite, which is higher than the value for hematite and nearest to our value.

Other physical parameters related with the electronic and magnetic properties of bulk goethite were calculated to investigate their dependence with U_{eff}. In Fig. 3(b) and (c) the results of the band gaps and magnetic moments for bulk goethite performed at LDA + U and GGA + U levels are shown, respectively. The band gap for bulk goethite is the lowest energy transition from the top of the valence band, mainly formed by O(2p), to the bottom of the conduction band

containing mostly Fe(3*d*) and this condition must be well represented in any theoretical approach. In order to determine this parameter for each optimized structure, the DOS projected onto Fe(3*d*) and O(2*p*) atomic orbitals were calculated. From Fig. 3(b) we notice that as the on-site Coulomb interaction increases, the band gap prediction is greatly improved. This behavior was corroborated at both LDA + *U* and GGA + *U* levels. The values obtained at GGA + *U* level are higher than the corresponding at LDA + *U*. To our knowledge, two experimental results for the goethite band gap are available in the range of 2.1–2.5 eV [59,60]. Regarding the results of Fig. 3(c) corresponding to the local magnetic moments on Fe atoms, we observe that at standard LDA level the magnetic moment is close to 1 μ_B, while with the inclusion of the on-site repulsion term, its value increases up to 4.5 μ_B. At standard GGA level, the magnetic moment on Fe ions is clearly higher (3.6 μ_B) than that obtained at standard LDA level. The local magnetic moments on Fe atoms also increase with the addition of the on-site repulsion term, reaching values up to 4.5 μ_B. In the published literature there is only one experimental result of the Fe magnetic moment, with a value of 3.80 μ_B for fine-particle goethite [61].

Therefore, and from this analysis, can infer that using GGA + *U* with U_{eff} = 6.0 eV we have also a reasonable representation of both the electronic and magnetic properties of bulk goethite.

In Fig. 4(a) the LDOS calculated at LDA + *U* level with U_{eff} = 0 eV (standard LDA) and U_{eff} = 6 eV are plotted, while in Fig. 4(b), we have the corresponding LDOS at GGA + *U* level. The standard LDA results show a strong mixing between the majority (or spin-up) and minority (or spin down) Fe(3*d*) states near the Fermi level, with a portion of majority states above and a contribution of minority states below this level. The observation of a peak below the Fermi level corresponding to the minority Fe(3*d*) can be associated with the existence of Fe(II) ions. The distribution of electronic states at the standard LDA level is spread, while the distribution becomes much localized when the on-site repulsion term is included. At the LDA + *U* level with U_{eff} = 6 eV, the top of valence band is composed predominantly by O(2*p*) states and the bottom of the conduction band is mainly formed by the unoccupied minority Fe(3*d*) states. Moreover, the majority Fe(3*d*) states are completely occupied, which is consistent with the Fe(III) oxidation state. The distribution of states is more localized at the standard GGA level than at the standard LDA, with the majority Fe(3*d*) states mainly occupied below the Fermi level and the minority Fe(3*d*) states mainly unoccupied above this level; nevertheless the predicted band gap is badly represented. At the GGA + *U* level with U_{eff} = 6 eV, the majority and minority Fe(3*d*) states are pushed at lower and higher energy values, respectively, and the energy difference between the highest occupied orbital (O(2*p*) states) and the lowest unoccupied orbital (minority Fe(3*d*) states) is increased. Consequently, the goethite electronic structure has clearly Fe(III) ions.

Local atomic charges have been calculated with the atoms-in-molecules-analysis due to Bader [62] using a fast algorithm developed by Henkelman et al. [63,64]. At the same U_{eff}, the atomic charges are higher for GGA + *U* than for LDA + *U* level. As the U_{eff} values increase, the atomic charges for all the atoms increase monotonously. This behavior is more pronounced from U_{eff} = 3 eV to U_{eff} = 5 eV; for larger values of U_{eff} Bader charges are only slightly modified, reaching values near to 2.0 *e* for the Fe atoms. From these results, together with the magnetic moments on Fe ions and the DOS analysis, we can conclude that the inclusion of the on-site repulsion term to the Kohn–Sham Hamiltonian (U_{eff}) is essential to identify bulk goethite like a Fe(III) compound.

3.2. Bulk Al-rich goethite

As it was above mentioned, Al-rich goethite may present a substitution of up to 33 mol% of Fe sites. The influence of Al on

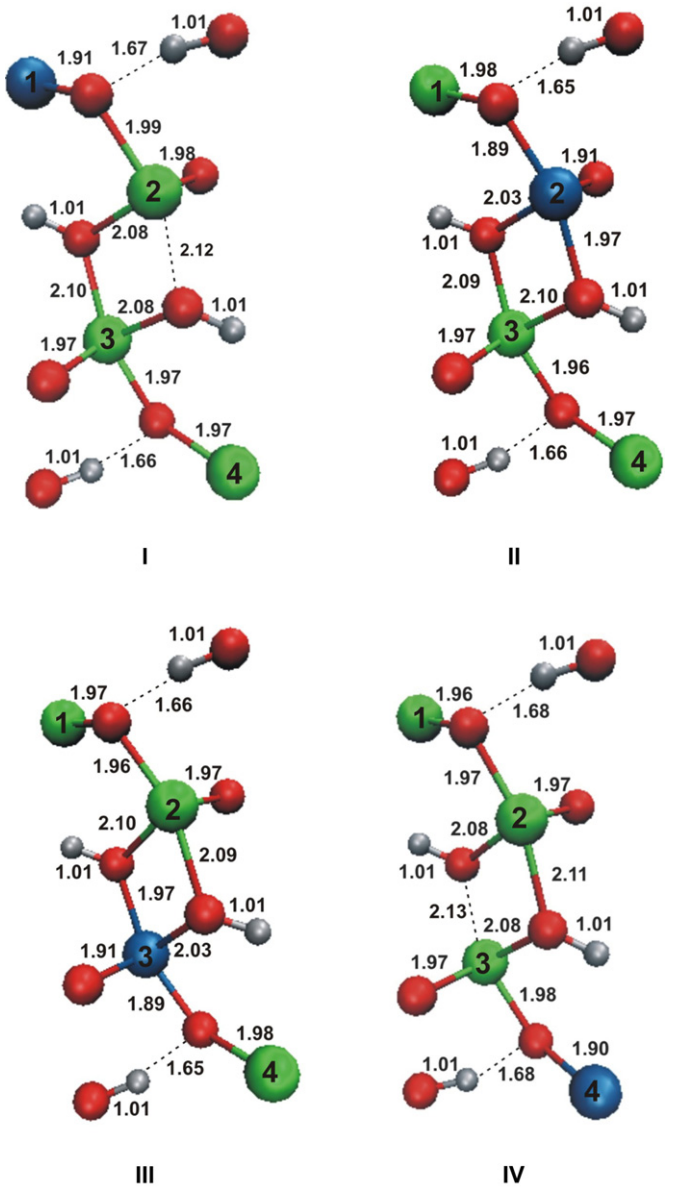

Fig. 5. Al-rich goethite geometries obtained with GGA + *U* (U_{eff} = 6 eV). Blue ball corresponds to Al atom. Distances between atoms are expressed in Armstrongs (Å). (For interpretation of the references to color in this figure legend, the reader is referred to the web version of this article.)

Mössbauer spectrum of substituted goethite was firstly observed forty years ago [65]. Since that time, some other experiments with Al-doped goethite were performed. J. Fleisch et al. [16] found that in goethite with a 12 mol% of Al-substitution the Néel temperature decreases below the room temperature, while for an Al-substitution higher than 15% this parameter shows a non-linear variation with Al content. In a subsequent work the magnetic ordering of two bulk Al-rich goethites with different crystal sizes and crystallinities was experimentally investigated by E. Murad and L.H. Bowen [66]. These authors found that the Néel temperature was different depending on the local composition inhomogeneities at an atomic scale of the Al–goethites, giving different magnetic configurations. It was shown that the samples with poor crystallinity must be cooled down to significantly lower temperatures to attain a complete magnetic order. In another work [67] it was evidenced that the presence of Al atoms in fine goethite particles causes an

Table 1
Lattice parameters (in Å), bulk moduli (in GPa) and cell volume (V, in Å^3) for bulk Al–goethite obtained with GGA(PW91) + U with U_{eff} = 6 eV. The magnetic configurations are indicated by the spin projection of Fe atoms in the unit cell. Different unit cell parameters from experiments were included for comparison.

Al structure – Mol% Al	Magnetic configuration	a	b	c	Bulk modulus	V
Al_I–a	**Al**/Fe(↓)/Fe(↑)/Fe(↓)	4.556	9.881	2.990	136	134.6
Al_I–b	**Al**/Fe(↑)/Fe(↓)/Fe(↑)	4.556	9.880	2.989	140	134.6
Al_{II}–a	Fe(↑)/**Al**/Fe(↑)/Fe(↓)	4.557	9.881	2.990	136	134.7
Al_{II}–b	Fe(↓)/**Al**/Fe(↓)/Fe(↑)	4.557	9.882	2.990	141	134.7
Al_{III}–a	Fe(↑)/Fe(↓)/**Al**/Fe(↓)	4.557	9.881	2.990	135	134.6
Al_{III}–b	Fe(↓)/Fe(↑)/**Al**/Fe(↑)	4.556	9.880	2.989	137	134.6
Al_{IV}–a	Fe(↑)/Fe(↓)/Fe(↑)/**Al**	4.563	9.879	2.990	133	134.8
Al_{IV}–b	Fe(↓)/Fe(↑)/Fe(↓)/**Al**	4.566	9.874	2.991	134	134.9
25% – theoretical [67]	Antiferromagnetic	4.591	9.948	3.017		137.8
25% – Vegard's law [67]		4.577	9.820	2.986		134.3
17.3 [64]		4.638	9.866	2.997		
20.0 [63]		4.593	9.848	2.990		
24.4 [65]		4.619	9.827	2.983		
24.9 [11]		4.622	9.882	2.978		
26.1 [62]		4.560	9.830	2.977		

The position of Al atom is marked with bold font.

imbalance of Fe magnetism, which results in particles with a net ferrimagnetic moment. The complexity of the magnetic configuration on Al-rich goethites was clearly evidenced in these experiments.

Taking into account the experimental data, we decided to make an isomorphous replacement of one Fe atom by one Al atom in the unit cell giving an Al-substitution of 25%. The lattice parameters previously obtained with GGA + U (U_{eff} = 6 eV) for bulk goethite were used as a starting point in the optimization of the unit cells of Al-doped goethite. Due to the complexity of the magnetic structures on Al-rich goethites, two situations for the magnetic ordering were considered, i.e., an antiferromagnetic phase (like bulk goethite) and a magnetic ordering where the spin projections of the Fe atoms were unconstrained. Our results indicated that the antiferromagnetic phase is 3 eV less stable than the second situation. Thus, all the results showed here correspond to the last magnetic phase.

In order to study in more detail the different geometrical arrangements and inherent magnetic configurations the Al-position was changed within the unit cell. The resulting geometrical position was named as I, II, III and IV according to replacement of a Fe atom in the unit cell by an Al atom (see Fig. 5). For each Al-position, different initial magnetic configurations for the three remaining Fe atoms were evaluated, changing the position of up and down local spin projections within the cell. The resulting most stable magnetic arrangements of Fe atoms were those with the same spin projection for the two Fe atoms surrounding the Al atom. The metal atoms are arranged in chains along the c-vector axis, each unit of the chain being constituted by two adjacent octahedrons.

The lattice parameters, bulk moduli and cell volumes of these situations are summarized in Table 1. As it is expected, the isomorphic substitution of Fe by Al in bulk goethite results in a lattice contraction due to the smaller radius of Al^{3+} ion with respect to Fe^{3+} ion (~0.1 Å). The contractions are of almost 0.05 Å, 0.07 Å and 0.04 Å for a, b and c cell parameters, respectively, and they are between the experimental data [68–71]. The lattice parameters obtained from the experiments are greatly dispersed, because they are strongly dependent on the Al amount incorporated into the goethite structure and the synthesis conditions [11,72]. The b and c parameters decrease linearly with the

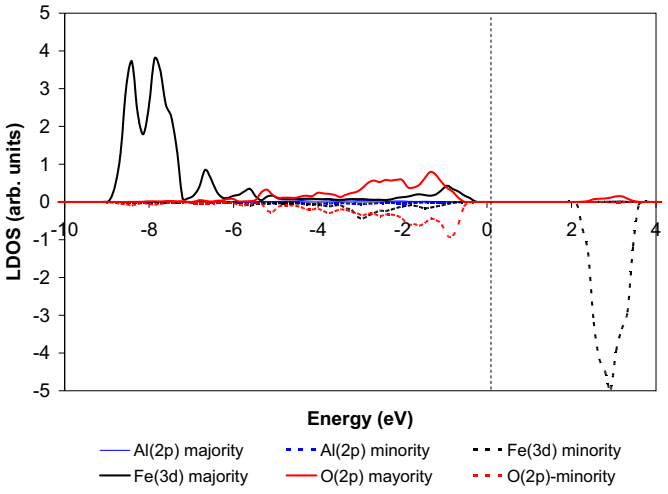

Fig. 6. LDOS localized on Fe, Al and O atoms for Al-rich goethite with GGA + U (U_{eff} = 6 eV). Negative numbers on the LDOS axis indicate the spin-down polarization.

Al-substitution, but not the a-parameter. This behavior can be associated with the strong link present in the b–c plane through a shared edge between two octahedra of the chain, while the neighboring chains along the a-vector interact only through shared apical oxygen and hydrogen bonds. It is notable that the OH concentration is highly dependent of experimental conditions during crystal growth. From Vegard's law, which assumes that a linear relationship exists between the size of the unit cell of the binary oxide and those of pure goethite and pure diaspore [8], it is possible to obtain experimentally the predicted lattice parameters at 25 mol% Al. However, some experimental data showed that the atomic parameters did not obey the Vegard's law for solid solutions with Al amount higher than 20%, specially the a-parameter [8,72].

In particular, our cell parameter values are in agreement with different experimental data summarized in Table 1 at nearly 25 mol % Al. Looking at the experimental results of Ref. [8], which are the closest to the 25% substitution, our results are in very good agreement with only discrepancies of −0.07, 0.00 and +0.01 Å, for a, b and c parameters, respectively. The higher difference was of 1.4% for the first of them, which becomes the most altered parameter by the experimental conditions. Comparing with respect to Vegard's values the higher difference was of 0.6%. In our model, the Al atoms are distant one each other by 2.99 Å, forming an Al chain in the c direction. EXAFS results indicated that Al atoms tend to cluster along the single octahedral chains [72].

Recently, a DFT study using a periodic model for bulk Al–goethite was performed [19]. In that publication, two models of Al substituted goethite with a clustered arrangement of Al atoms within the goethite structure were considered. These models with 8 and 25 mol% of Al predicted better the unit cell parameters than an isolated Al arrangement. The isolated Al arrangement contains the Al atoms at a longer distance (6.73 Å) than the Al-clustered arrangement (3.15 Å). The last case is similar to our model.

From the DOS analysis, we obtained a band gap value of 2.0 eV for all the magnetic configurations presented in Table 1. Besides, the bulk modulus is predicted to be around 137 GPa. To our knowledge, no experimental values were previously reported for these properties. Fig. 6 shows the calculated LDOS for Al-rich goethite. It is possible to observe that the electron DOS distributions of Fe and O atoms are similar to that obtained for goethite. The valence states of Al atom are practically absent for energies below the Fermi level, indicating that this atom exhibits an Al^{3+} ionic character.

The values of the magnetic moments on Fe atoms are maintained with respect to the pure goethite, but some O atoms,

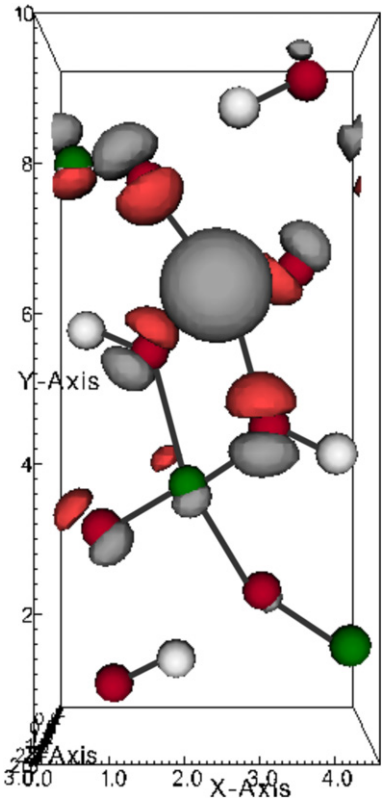

Fig. 7. Charge density difference between goethite and Al-rich goethite obtained with GGA + U (U_{eff} = 6 eV). Gray and red isosurfaces correspond to the depleted and the gained electronic charge, respectively. (For interpretation of the references to color in this figure legend, the reader is referred to the web version of this article.)

especially those which are directly bonded to an Al atom, have a slight magnetization ($\sim$0.1 μ_B). The atomic Bader charges indicate that both Al and Fe ions have +3 oxidation state. The oxygen atoms surrounding the Al ions have an additional negative charge with respect to the pure goethite (O: −1.60 *e* and OH: −1.83 *e*). This fact can be observed in the spatial distribution of the charge density difference between goethite and Al-rich goethite (see Fig. 7). The zone surrounding the Al ion undergoes a depletion of electronic charge, while the zones surrounding the O ions directly linked with it present both a reduction and an increment of electronic charge. In these cases, the gained electron charge is slightly higher than that lost one and, this fact can be associated with the appearance of a net magnetization on these ions.

As an estimation of energy cost to create our Al–goethite system with respect to the pure goethite, we considered the energy balance for the substitution of a Fe atom of the goethite by an Al atom, as expressed in equation (1):

$$\text{Goethite} + \text{Al atom} \rightarrow \text{Al–goethite} + \text{Fe atom}$$

$$E = \left(E_{\text{Al–goethite}} + E_{\text{Fe atom}}\right) - \left(E_{\text{goethite}} - E_{\text{Al atom}}\right) \quad (1)$$

This energy difference accounts for the affinity of goethite system towards the exchange of one Fe atom by one Al atom. Regarding the electronic configurations for the isolated atoms Fe and Al used in equation (1), they correspond to Fe d^7s^1 and Al s^2p^1, respectively. The computed E value is −3.56 eV, indicating that the reaction is an exothermic process. Estimated zero-point energy corrections do not alter these energy affinity results. This result indicates an important affinity to obtain the Al–goethites, as it was found in the open literature [8,11].

Table 2
Harmonic vibrational frequencies (in cm^{-1}) for bulk goethite and bulk Al–goethite obtained with GGA(PW91) + U_{eff} = 6 eV.

	ν (O–H)	δ (O–H) in a–b plane	δ (O–H) out a–b plane	ν (Fe–O)
Goethite	3027–3000	1099–1023	1001–998 941	635
Al–goethite	2980–2953[a]	1153 (Al–OH)	1068 (Al–OH)	659 (Al–O)
	2977–2895[b]	1129 (Fe–OH)	1014 (Fe–OH)	629 (Fe–O)
Goethite Exp. [4,73,74]	3170–3085	890	795	640–620

[a] O–H group linked to Al and Fe atoms.
[b] O–H group linked to two Fe atoms.

3.3. Vibrational frequencies

Moreover, a comparative study of the vibrational frequencies of bulk goethite and Al-doped goethite was performed. Only the vibrational modes which can be compared with experimental data were presented in Table 2. Our results predict for bulk goethite a band in the range of 3027–3000 cm^{-1} containing the stretching frequencies of the four bulk hydroxyls, which vibrate in different coupled or uncoupled modes. Other band appears at 1099–1023 cm^{-1} due to the O–H bending vibrations in the a–b plane, while the O–H bending out of the plane are at 1001–998 cm^{-1} and 941 cm^{-1}. A frequency obtained at 635 cm^{-1} corresponds to the Fe–O stretching. Experimental FTIR results for pure goethite are scarce, nevertheless, the FTIR spectra of goethite contain four main features that could be related to our calculations: an intense band in the range of 3170–3085 cm^{-1} corresponding to the O–H stretching, four peaks at about 890 cm^{-1} and 795 cm^{-1} due to the OH bending vibrations in and out of the a–b plane, respectively, and a band in the range of 640–620 cm^{-1} corresponding to the Fe–O stretching vibrations [4,73,74]. These assignments were made considering that the experimental spectra are not largely distorted by temperature dependent effects, as is it usually assumed in the literature [31,75–77]. It is outstanding that P. Cambier [78] found that the decreasing O–H stretching frequencies and the increasing O–H bending frequencies can be related with a crystalline order and the cell parameters. It is reasonable to consider that the OH band displacements correspond to an enhancement of the H-bond strength [79]. Mainly, the H-bond strength changes due to the decreasing a-parameter. These results explain our lower O–H stretching frequency and our higher O–H bending frequencies with respect to the experimental data previously mentioned, due to the lower a-parameter in our bulk goethite model.

When the goethite is doped with Al the unit cell parameters are contracted and this fact produces changes in bond distances and angles, modifying the frequency positions in comparison with pure goethite. Indeed, the symmetry of the unit cell is broken and more features appear in the spectrum, due particularly to the stretching and bending modes of the hydroxyl linked with Fe and Al ions. The positions of the hydroxyl stretching bands are in the ranges of 2980–2953 cm^{-1} for the O–H groups bonded to Al and Fe and of 2977–2895 cm^{-1} for the O–H bonded to two Fe atoms. The frequencies for the O–H bending in the plane are located at 1153 (Al–OH) and 1129 (Fe–OH) cm^{-1}, while those for the O–H bending out of the plane are at 1068 (Al–OH) and 1014 (Fe–OH) cm^{-1}. Finally, the frequencies for the Me–O stretching

modes appear at 659 cm^{-1} for Me = Al and at 629 cm^{-1} for Me = Fe. Summarizing, the O–H stretching bands are located at lower frequency values than in pure goethite, while the O–H bending and Me–O stretching modes are located at higher frequency values. Besides, the Me–O stretching frequencies also increase their values.

Experimentally, the presence of Al in bulk goethite produces analogous shifts in IR bands together with the broadening of the spectral peaks due to the different atomic environments [80]. Stiers and Schwertmann [81] also reported shifts in the O–H bending band to higher frequencies with increasing substitution of Mn^{3+} or Al^{3+} for Fe^{3+} in goethite. Subsequently, a similar behavior was observed when the pure goethite was exposed under different pressures [73]. These interesting results indicate that pressure induces changes and a reorientation of the hydroxyl bonding, modifying its bending vibration. The O–H bending out of the plane is the most altered signal with the external pressure. The shift of hydroxyl bending bands is due to the non-linear hydrogen bond, –Fe–**O**–**H**…**O**–Fe, with respect to the oxygen–oxygen axis. The reason of this bending is the larger repulsion between the hydrogen ion and the neighboring cationic ions [73] due to the smaller H-ion distances. Indeed, in our bulk goethite the nearest neighboring Fe ions are at 2.64 Å and 2.98 Å, while the H-ion distances in bulk Al-rich goethite are 2.53 Å and 2.92 Å with respect to Fe and Al ions, respectively. The H-bonding has a length of 1.69 Å and 1.67 Å for goethite and Al–goethite, respectively. Finally, an increase in the Fe–O stretching frequency could be the main evidence for Al/Fe substitutions [78].

The above performed calculations help us to ensure that the bulk goethite and Al-doped goethite are well descripted. As it was previously mentioned by Illas et al. [36], the election of an optimal U_{eff} parameter considering a large set of experimental data is an efficient way to study complex systems within the DFT + U formalism. From the presented results, we could generate different surfaces of goethite and Al-doped goethite with the certainty that the model will reproduce the chemical reactivity of these systems.

4. Conclusions

The theoretical study of bulk goethite performed in this work, with a careful consideration of the correlation effects due to the more localized 3d-electrons of Fe, shows that the GGA + U method of DFT describes more adequately than the LDA + U one the structural and electronic properties of this oxide. The use of $U_{eff} = 6$ eV is the better choice regarding properties such as lattice constants, bulk moduli, density of states, magnetic moments and atomic charges. The calculation of magnetic moments of Fe ions, the DOS analysis and the Bader atomic charges identifies the goethite, in agreement with experiments, as an antiferromagnetic Fe(III) compound. The subsequent extension of this approach to Al-rich goethite using a model where 25% of Fe was substituted shows that four magnetic orderings can be found, all of them with similar energies. In these orderings the Fe atoms surrounding the Al atom must have the same spin projection, i.e., spin-up or -down. The unit cell parameters of the Al-doped goethite are in complete agreement with the experimental result for similar Al content. The isomorphic substitution of Fe by Al in goethite results in a lattice contraction due to the smaller radius of $A1^{3+}$ ion with respect to Fe^{3+} ion. This Al-rich goethite model presents the Al ions forming a chain along the c-vector axis. Local charge redistribution is observed surrounding each Al ion, where the O atoms exhibit small additional negative charges with respect to the pure goethite. This feature could change the adsorption capability of the Al–goethite surfaces.

Acknowledgments

This research was carried out for the financial support of CONICET, ANPCYT and Universidad Nacional del Sur.

References

[1] T. Hahn (Ed.), International Tables of Crystallography, Kluwer Academic Publishers, Norwell, MA, 1996.
[2] J.B. Forsyth, I.G. Hedleys, C.E. Johnson, J. Phys. C (Proc. Phys. Soc.) 1 (1968) 179.
[3] R. Morris, G. Klingelhofer, B. Bernhardt, C. Schroder, D. Rodionov, P. de Souza Jr., A. Yen, R. Gellert, E. Evlanov, J. Foh, E. Kankeleit, P. Gutlich, D. Ming, F. Renz, T. Wdowiak, S. Squyres, R. Arvidson, Science 305 (2004) 833.
[4] U. Schwertmann, P. Cambier, E. Murad, Clays Clay. Miner. 33 (1985) 369.
[5] T. Nagai, H. Kagi, T. Yamanaka, Am. Miner. 88 (2003) 1423.
[6] A.E. Gleason, R. Jeanloz, M. Kunz, Am. Miner. 93 (2008) 1882.
[7] S. Sepulveda-Guzman, O. Perez-Camacho, O. Rodriguez-Fernandez, J. Magn. Magn. Mat. 294 (2005) 47.
[8] D.G. Schulze, U. Schwertmann, Clay. Miner. 19 (1984) 521.
[9] E. Wolska, Adv. Soil Ecol. 30 (1997) 271.
[10] M. Álvarez, E.H. Rueda, E.E. Sileo, Geoderma 140 (2007) 8.
[11] D.G. Schulze. and reference therein, Clays Clay. Miner. 32 (1984) 36.
[12] J. Majzlan, A. Navrotsky, Eur. J. Miner. 15 (2003) 495.
[13] A.J. Blanch, J.S. Quinton, C.E. Lenehan, A. Pring, Miner. Mag. 72 (2008) 1043.
[14] H.D. Ruan, R.J. Gilkes, Clays Clay. Miner. 2 (1995) 196.
[15] U. Schwertmann, H. Stanjek, Clays Clay. Miner. 3 (1998) 317.
[16] J. Fleisch, R. Grimm, J. Grtibler, P. Giitlich, J. Physique 4l Cl (1980) 169.
[17] M. Mohapatra, K. Rout, S. Anand, J. Hazard. Mat. 171 (2009) 417.
[18] S. Liao, J. Wang, D. Zhu, L. Ren, J. Lu, M. Geng, A. Langdon, Appl. Clay. Sci. 38 (2007) 43.
[19] E. Bazilevskaya, D.D. Archibald, M. Aryanpour, J.D. Kubicki, C. Enid Martínez, Geochim. Cosmochim. Acta (2011). http://dx.doi.org/10.1016/j.gca.2011.05.041.
[20] B. Winkler, M. Hytha, C. Pickard, V. Milman, M. Warren, M. Segall, Eur. J. Miner. 13 (2001) 343.
[21] A.C.Q. Ladeira, V.S.T. Ciminelli, H.A. Duarte, M.C.M. Alves, A.Y. Ramos, Geochim. Cosmochim. Acta 65 (2001) 1211.
[22] T.H. Yoon, S.B. Johnson, C.B. Musgrave, G.E. Brown Jr., Geochim. Cosmochim. Acta 68 (2004) 4505.
[23] G. Rollmann, A. Rohrbach, P. Entel, J. Hafner, Phys. Rev. B 69 (2004) 165107.
[24] S. Yin, D.E. Ellis, Surf. Sci. 603 (2009) 736.
[25] K.W. Paul, J.D. Kubicki, D.L. Sparks, Eur. J. Soil Sci. 58 (2007) 978.
[26] D.M. Sherman, S.R. Randall, Geochim. Cosmochim. Acta 67 (2003) 4223.
[27] N.H. de Leeuw, T.G. Cooper, Geochim. Cosmochim. Acta 71 (2007) 1655.
[28] A.J.A. Aquino, D. Tunega, G. Haberhauer, M.H. Gerzabek, H. Lischka, Geochim. Cosmochim. Acta 72 (2008) 3587.
[29] R. Rahnemaie, T. Hiemstra, W.H. van Riemsdijk, J. Colloid Interface Sci. 315 (2007) 415.
[30] A.J.A. Aquino, D. Tunega, G. Haberhauer, M.H. Gerzabek, H. Lischka, J. Phys. Chem. C 111 (2007) 877.
[31] K.D. Kwon, J.D. Kubicki, Langmuir 20 (2004) 9249.
[32] B. Russell, M. Payne, L.C. Ciacchi, Phys. Rev. B 79 (2009) 165101.
[33] H. Guo, A.S. Barnard, Phys. Rev. B 83 (2011) 094112.
[34] N. Hamdad, B. Bouhafs, Physica B 405 (2010) 4595.
[35] N. Hamdad, Physica B 406 (2011) 1194.
[36] Ch. Loschen, J. Carrasco, K.M. Neyman, F. Illas, Phys. Rev. B 75 (2007) 035115.
[37] M. Cococcioni, S. de Gironcoli, Phys. Rev. B 71 (2005) 035105.
[38] H.J. Kulik, M. Cococcioni, D.A. Scherlis, N. Marzari, Phys. Rev. Lett. 97 (2006) 103001.
[39] G. Mattioli, F. Filippone, P. Alippi, A. Amore Bonapasta, Phys. Rev. B 78 (2008) 241201.
[40] S. Lisenkov, I.A. Kornev, L. Bellaiche, Phys. Rev. B 79 (2009) 012101.
[41] B.J. Morgan, G.W. Watson, J. Phys. Chem. C 113 (2009) 7322.
[42] H. Hsu, K. Umemoto, M. Cococcioni, R. Wentzcovitch, Phys. Rev. B 79 (2009) 125124.
[43] Y. Jiang, J.B. Adams, M. van Schilfgaarde, J. Chem. Phys. 123 (2005) 064701.
[44] M. Nolan, S. Grigoleit, D.C. Sayle, S.C. Parker, G.W. Watson, Surf. Sci. 576 (2005) 217.
[45] A. Rohrbach, J. Hafner, G. Kresse, J. Phys. Condens. Matter 15 (2003) 979.
[46] G. Kresse, J. Hafner, Phys. Rev. B 47 (1993) 558.
[47] G. Kresse, J. Hafner, Phys. Rev. B 48 (1993) 13115.
[48] G. Kresse, J. Hafner, Phys. Rev. B 49 (1994) 14251.
[49] P. Blöchl, Phys. Rev. B 50 (1994) 17953.
[50] G. Kresse, D. Joubert, Phys. Rev. B 59 (1999) 1758.
[51] S.L. Dudarev, G.A. Botton, S.Y. Savrasov, C.J. Humphreys, A.P. Sutton, Phys. Rev. B 57 (1998) 1505.
[52] J.P. Perdew, J.A. Chevary, S.H. Vosko, K.A. Jackson, M.R. Pederson, D.J. Singh, C. Fiolhais, Phys. Rev. B 46 (1992) 6671.
[53] J.P. Perdew, J.A. Chevary, S.H. Vosko, K.A. Jackson, M.R. Pederson, D.J. Singh, C. Fiolhais, Phys. Rev. B 48 (1993) 4978.
[54] B. Meredig, A. Thompson, H.A. Hansen, C. Wolverton, Phys. Rev. B 82 (2010) 195128.
[55] A.I. Liechtenstein, V.I. Anisimov, J. Zaanen, Phys. Rev. B 52 (1995) R5467.

[56] A. Szytula, A. Burewicz, Z. Dimitrijewic, S. Krasnicki, H. Rzany, J. Todorovic, A. Wanic, W. Wolski, Phys. Status Sol. 26 (1968) 429.
[57] G.A. Waychunas, C.C. Fuller, B.A. Rea, J.A. Davis, Geochim. Cosmochim. Acta 60 (1996) 1765.
[58] J.D. Kubicki, K.W. Paul, D.L. Sparks, Geochem. Trans. 9 (2008) 4.
[59] J.K. Leland, A.J. Bard, J. Phys. Chem. 91 (1987) 5076.
[60] D.M. Sherman, Geochim. Cosmochim. Acta 69 (2005) 3249.
[61] S. Bocquet, S.J. Kennedy, J. Magn. Magn. Mat. 109 (1992) 260.
[62] R.F.W. Bader, Atoms in Molecules: A Quantum Theory, Oxford Science, Oxford, UK, 1990.
[63] G. Henkelman, A. Arnaldsson, H. Jónsson, Comput. Mater. Sci. 36 (2006) 254.
[64] E. Sanville, S.D. Kenny, R. Smith, G. Henkelman, J. Comput. Chem. 28 (2007) 899.
[65] C. Janot, G. Gubert, Bulletin de la Société française de Minéralogie et Cristallographie 93 (1970) 213.
[66] E. Murad, L.H. Bowen, Am. Miner. 72 (1987) 194.
[67] R.J. Pollard, Q.A. Pankhurst, P. Zientek, Phys. Chem. Miner. 18 (1991) 259.
[68] R. Thiel, Anorg. Allg. Chem. 326 (1963) 70.
[69] P.G. Fazey, B.H. O'Connor, L.C. Hammond, Clays Clay. Miner. 39 (1991) 248.
[70] Q. Liu, Y. Yu, J. Torrent, A.P. Roberts, Y. Pan, R. Zhu, J. Geophys. Res. 111 (2006) B12S34.
[71] K. Jónás, K. Solymár, Acta Chim. Acad. Sci. Hung. 66 (1970) 383.
[72] J.L. Hazemann, J.F. Bèrar, A. Manceau, Mat. Sci. Forum 79-82 (1991) 821.
[73] Q. Williams, L. Guenther, Solid State Commun. 100 (1996) 105.
[74] L.C.A. Oliveira, T.C. Ramalho, E.F. Souza, M. Gonçalves, D.Q.L. Oliveira, M.C. Pereira, J.D. Fabris, Appl. Catal. B 83 (2008) 169.
[75] N. Zhang, P. Blowers, J. Farrell, Environ. Sci. Technol. 39 (2005) 4816.
[76] M. Zhang, G. He, G. Pan, J. Colloid Interface Sci. 338 (2009) 284.
[77] S.M. Kozlov, G.F. Cabeza, K.M. Neyman, Chem. Phys. Lett. 506 (2011) 92.
[78] P. Cambier, Clay. Miner. 21 (1986) 201.
[79] G.C. Pimentel, A.L. MacClellan, The Hydrogen Bond, Freeman and Co., San Francisco & London, 1960.
[80] S.A. Fysh, P.M. Fredericks, Clays Clay. Miner. 31 (1983) 377.
[81] W. Stiers, U. Schwertmann, Geochim. Cosmochim. Acta 49 (1985) 1909. 20.
[82] J.R. Rustad, A.R. Felmy, B.P. Hay, Geochim. Cosmochim. Acta 60 (1996) 1563.